Parallel regulation of thyroid hormone transporters OATP1c1 and MCT8 during and after endotoxemia at the blood-brain barrier of male rodents

Gábor Wittmann[1], Judit Szabon[2], Petra Mohácsik[2,3], Shira S. Nouriel[1], Balázs Gereben[2], Csaba Fekete[1,2] and Ronald M. Lechan[1,4]

[1]Department of Medicine, Division of Endocrinology, Diabetes and Metabolism, Tupper Research Institute, Tufts Medical Center, Boston, MA 02111

[2]Department of Endocrine Neurobiology, Institute of Experimental Medicine, Hungarian Academy of Sciences, Budapest 1083, Hungary

[3]Semmelweis University, János Szentágothai PhD School of Neurosciences, Budapest, 1085 Hungary

[4]Department of Neuroscience, Tufts University School of Medicine, Boston, MA 02111

Abbreviated title: Regulation of OATP1c1 and MCT8 by LPS

Keywords: organic anion transporting polypeptide, monocarboxylate transporter, lipopolysaccharide

Word count: 4512

Corresponding author and to whom reprint requests should be addressed:

Gábor Wittmann, PhD or Ronald M. Lechan, MD, PhD

Department of Medicine, Division of Endocrinology, Diabetes and Metabolism

Tufts Medical Center, #268

800 Washington Street

Boston, Massachusetts, 02111

Phone: 617-616-8514

Fax: 617-636-4719

E-mail: gwittmann@tuftsmedicalcenter.org or rlechan@tuftsmedicalcenter.org

This work was supported by NIH grant DK-37021, a grant from the Dr. Gerald J. and Dorothy R. Friedman New York Foundation for Medical Research, EU FP7 contract Switchbox (Grant n° 259772), the Hungarian National Brain Research and Lendület Programs and OTKA109415.

Disclosure summary: The authors have nothing to disclose

Abstract

There is increasing evidence that local thyroid hormone (TH) availability changes profoundly in inflammatory conditions due to altered expression of deiodinases that metabolize TH. It is largely unknown, however, how inflammation affects TH availability *via* the expression of TH transporters. In this study we examined the effect of bacterial lipopolysaccharide (LPS) administration on two TH transporters that are critically important for brain TH homeostasis, organic anion-transporting polypeptide 1c1 (OATP1c1) and monocarboxylate transporter 8 (MCT8). Messenger RNA levels were studied by *in situ* hybridization and quantitative PCR, and protein levels by immunofluorescence in both the rat and mouse forebrain. The mRNA of both transporters decreased robustly in the first 9h after LPS injection, selectively in brain blood vessels; OATP1c1 mRNA in astrocytes and MCT8 mRNA in neurons remained unchanged. At 24 and/or 48h after LPS administration, OATP1c1 and MCT8 mRNAs increased markedly above control levels in brain vessels. OATP1c1 protein decreased markedly in vessels by 24h, whereas MCT8 protein levels did not decrease significantly. These changes were highly similar in mice and rats. The data demonstrate that OATP1c1 and MCT8 expression are regulated in a parallel manner during inflammation at the blood-brain barrier of rodents. Given the indispensable role of both transporters in allowing TH access to the brain, the results suggest reduced brain TH uptake during systemic inflammation.

Introduction

It is well known that thyroid hormone (TH) homeostasis is altered in association with acute and chronic illnesses, a disorder commonly referred to as the nonthyroidal illness syndrome and manifested by reduced serum TH levels and an inappropriately low TSH (1-3). However, there is limited understanding about how TH availability changes at the level of specific target cells and tissues under these conditions. Local TH availability is largely determined by the presence of TH transporters that enable the passage of TH across cellular membranes, and deiodinases that metabolize TH (4, 5). Deiodinases have been studied extensively in animal models of inflammatory conditions (1), particularly type 2 deiodinase (D2) that activates T4 to the biologically more potent T3 (4). In these models, D2 expression increases in several organs (6-15), including novel expression in cells and tissues where it is not normally present (6, 8, 15), suggesting a local anti-inflammatory role for TH (6, 8, 16-18). In contrast, it is largely unknown how inflammation affects TH availability *via* TH transporters. Quantitative PCR studies reported decreased monocarboxylate transporter 8 (MCT8, coded by Slc16a2) expression in several organs of septic pigs (19) and in the subcutaneous fat of septic patients (20), while organic anion-transporting polypeptide 1c1 (OATP1c1, coded by Slco1c1) and monocarboxylate transporter 10 (MCT10) mRNAs increased in the hypothalamus of rabbits in prolonged critical illness (21). Details of these responses, such as cell-type specificity, temporal characteristics, and whether mRNA changes translate into protein levels, have not yet been studied. Shedding light on these aspects of TH handling would be important to better understand TH availability during disease at the cellular level.

Previously, we described how inflammation affects D2 expression in the brain of different rodent species, and demonstrated inflammation-induced D2 expression in the leptomeninges, choroid plexus and a subset of brain blood vessels (15). The present study was conducted to obtain a detailed, cell-type-specific insight into the inflammatory regulation of TH transporters. Of the several proteins capable of TH transport and present in the rodent brain (22, 23), we focused on OATP1c1 and MCT8 because they are critically important for brain TH homeostasis (24). Both transporters facilitate TH traffic in multiple cell

types (25-30), and are indispensable for TH entry into the brain *via* the blood-brain and/or blood-cerebrospinal fluid barrier (24, 31-34). In fact, almost the entire T3 uptake into the brain is facilitated by MCT8 (32), while both MCT8 and OATP1c1 contribute to T4 uptake (24). Importantly, a recent study by Mayerl et al. (24) demonstrated that the lack of both transporters results in a severely hypothyroid brain, with T3 and T4 contents being of only 10% of wild type levels.

In this study, we examined the effect of bacterial lipopolysaccharide (LPS) administration, an acute systemic inflammatory challenge, on OATP1c1 and MCT8 mRNA and protein expression in the brain using *in situ* hybridization, quantitative PCR, and immunofluorescence. Since we previously found major differences in the LPS-induced D2 expression between rats and mice (15), we performed the experiments in both species, with special attention to the rat meninges.

Materials and Methods

Animals

The experiments were carried out on adult, male, Sprague-Dawley (Taconic Farms) and Wistar rats (TOXI-COOP KKT, Hungary) weighing 220-260g, and adult, male C57Bl/6 mice (Taconic and Charles River), weighing 19-21 g. Animals were housed under standard conditions (lights on between 0600 and 1800 h, temperature 22 ± 1 C, rodent chow and water *ad libitum*). All experimental protocols were reviewed and approved by the Institutional Animal Care and Use Committee at Tufts Medical Center and the Animal Welfare Committee at the Institute of Experimental Medicine of the Hungarian Academy of Sciences.

Injections and tissue preparation

LPS-injections: Rats and mice were injected ip with LPS from *Escherichia coli* (serotype O55:B5; Sigma-Aldrich Co), dissolved in saline, at a dose of 2.5 mg/kg body weight to all animals according to the Guide of the American Thyroid Association (35). Control animals received the same volume of saline.

Experiment for quantitative PCR analysis: Groups of Wistar rats (n=6 per group) and C57Bl/6 mice (n=8 per group) were injected with LPS or saline, and were decapitated 9 or 48h later. The brains were dissected and samples from the cerebral cortex collected and stored at −80°C until subjected to real-time PCR. In another experiment, leptomeninges of the basal forebrain were collected from 6 control and 8 LPS-treated Sprague-Dawley rats 9h after the injections.

Time course experiment for in situ hybridization and immunofluorescence studies: Groups of Sprague-Dawley rats and C57Bl/6 mice (n=4 or 5 in each group) were injected with LPS and 2, 4, 9, 24 or 48h later were anesthetized with ketamine-xylazine, then decapitated. Control mice (n=5) were euthanized at 9h, and control rats were euthanized at 9h (n=3) or 24h (n=2), as *in situ* hybridization and immunofluorescent signals for OATP1c1 and MCT8 were of the same intensity in 9h and 24h control rat brains. The brains were removed, snap-frozen on powdered dry ice and 16 μm thick coronal sections were cut using a Leica CM3050 S cryostat (Leica Microsystems). Sections were thaw-mounted on Superfrost Plus slides (Fisher Scientific Co), air-dried and stored at -80°C until processed for *in situ* hybridization.

RNA isolation and Real time PCR analyses

RNA was isolated using the RNeasy Lipid Tissue Mini Kit (Qiagen) from cortex samples and with RNeasy Tissue Mini Kit (Qiagen) from leptomeninges according to the manufacturer's instructions. The purity and concentration of the RNA were analyzed using Spectrophotometer (Bio-Rad, SmartSpec Plus). Reverse transcription was performed with 1 μg of RNA to convert the total RNA to cDNA using the High Capacity cDNA Reverse Transcriptase Kit (Applied Biosystems by Life Technologies). Concentration of the generated cDNA was determined using the Qubit 2.0 Fluorometer with the Qubit ssDNA Assay Kit (Life Technologies). Expression of OATP1c1, MCT8 and D2 was measured by real-time quantitative TaqMan RT PCR reaction with a ViiA 7 Real-Time PCR System (Life Technologies), using commercially available TaqMan probes (code numbers are summarized in Supplementary Table 1.) on 10

ng cDNA template in duplicates. Glyceraldehyde-3-phosphate dehydrogenase (Gapdh) was used as housekeeping gene. Expression of the housekeeping gene did not vary between the experimental groups.

Generation of hybridization probes

Template cDNA fragments were generated with RT-PCR using standard procedures. Amplification was performed on cDNA synthesized from rat brain for OATP1c1 and mouse or rat liver for MCT8. Fragments were cloned into pGemT vector (Promega) and confirmed by sequencing. Probe sequences were as follows: rat OATP1c1 probe corresponds to nt 375-2525 of NM_053441.1 and has 93% homology with the corresponding mouse sequence, nt 368-2522 of NM_021471.2; mouse MCT8 probe nt 2569-3428 of NM_009197.2; rat MCT8 probe nt 41-648 of NM_147216.1, and has 98% homology with the mouse sequence NM_009197.2 between nt 227-834; rat D2 probe was reported previously (15). Antisense riboprobes were synthesized using SP6 or T7 RNA polymerase (Promega) in the presence of [35S]-uridine 5′-(alpha-thio) triphosphate (PerkinElmer), and purified with Mini Quick Spin RNA columns (Roche Applied Sciences). For fluorescent *in situ* hybridization, the OATP1c1 probe was labeled with digoxigenin-11-UTP (Roche).

Isotopic in situ hybridization

Isotopic *in situ* hybridization was performed as previously described (15, 36) using 50,000 cpm/µl radiolabeled probe concentrations. The same probe was used to detect OATP1c1 mRNA in both species; the rat MCT8 probe was used for rat sections, while both the rat and mouse MCT8 probes that are non-overlapping were used on mouse sections to increase hybridization sensitivity. Following stringency washes, sections were dehydrated in ascending ethanol series, air-dried, and placed on Amersham Hyperfilm autoradiography film (GE Healthcare Biosciences) for 6 days (rat OATP1c1) or 8 days (mouse OATP1c1 and MCT8). Slides were then dipped in Kodak NTB autoradiography emulsion (Carestream Health Inc), and stored at 4°C until developed. Exposure times were as follows: 9 days for mouse

OATP1c1; 24 days for mouse MCT8; two exposure times, 5 days and 9 days, were used for two different hybridizations for rat OATP1c1; 35 days for rat MCT8; and 14 days for rat D2. Autoradiograms were developed with Kodak D19 developer (Eastman Kodak Co). Sections were immersed in 0.0005% cresyl violet acetate (Sigma-Aldrich) for 2 min to obtain fluorescent labeling of cell nuclei, dehydrated in ascending ethanol series and xylenes, and coverslipped with DPX (Sigma-Aldrich). Darkfield images of the emulsion autoradiographs and fluorescent images of the cresyl violet signal were captured using a Zeiss Axioplan 2 microscope equipped with a SPOT Slider digital camera (Diagnostic Instruments).

Isotopic OATP1c1 in situ hybridization combined with GFAP immunofluorescence

Sections from the control and 9h LPS groups from both species were hybridized for OATP1c1 as above, then processed further for immunofluorescence. The sections were treated with the mixture of 0.5% Triton X-100 and 0.5% H_2O_2 for 15 min, rinsed in PBS (3×10 min), immersed in maleate buffer (pH 7.5) for 10 min, and then in 1% blocking reagent for nucleic acid hybridization (Roche). The sections were incubated overnight in a mouse monoclonal antibody against the astrocyte marker, glial fibrillary acidic protein (GFAP) (Cat# MAB360, Millipore, diluted 1:1,000), and subsequently in Alexa Fluor 488-conjugated donkey anti-mouse IgG (1:400; Life Technologies) for 2 hours. Sections were dehydrated and dipped in Kodak NTB autoradiography emulsion. The autoradiograms were developed after 9 days. The fluorescent signal of Alexa Fluor 488 was pseudo-colored to red for better visibility of dual-labeled cells.

Fluorescent OATP1c1 in situ hybridization combined with GFAP immunofluorescence

Hybridizations were performed on both fresh-frozen control rat sections, and sections from four normal paraformaldehyde-perfused rats. Paraformaldehyde-perfusion was performed as previously described (36). Briefly, rats were anesthetized with an overdose of pentobarbital (50 mg/kg) and perfused transcardially with PBS followed by 4% paraformaldehyde. The brains were postfixed by immersion in 4% paraformaldehyde, cryoprotected in 20% sucrose in PBS overnight, then snap-frozen on dry ice. Serial 20 μm coronal sections were cut on a cryostat, collected in cryoprotectant solution and stored at -

20°C until used. Fluorescent in situ hybridization for fresh-frozen and paraforaldehyde-perfused sections was performed as previously described (15, 36). The digoxigenin-labeled probe was detected with peroxidase-conjugated Fab fragments of sheep anti-digoxigenin antibody (1:100, Roche). The hybridization signal was amplified with biotinylated tyramide for 30 min using the TSA amplification kit (Perkin Elmer), and visualized by Alexa 488-conjugated Streptavidin (1:500; Life Technologies). Sections were reacted with murine GFAP antibody as above, and detected with Cy3-conjugated donkey anti-mouse IgG (Jackson ImmunoResearch). Sections were then coverslipped with Vectashield containing 4′,6-diamidino-2-phenylindole (DAPI) (Vector Laboratories).

Immunofluorescence for OATP1c1 and MCT8

For MCT8 immunofluorescence, mounted fresh-frozen sections were fixed with 4% paraformaldehyde in 0.1M phosphate buffer (pH 7.4) for 15 min. For OATP1c1 immunofluorescence, sections were fixed with methanol at −20°C for 5 min. Sections were permeabilized with 0.25% Triton-X-100 for 30 min, blocked with 2% normal horse serum in PBS, and incubated overnight in a rabbit antiserum against human MCT8 (raised against amino acids 527-539; #1306, gift from Dr. Theo J. Visser) or a rabbit antiserum against human OATP1c1 (raised against amino acids 697-712; #3516, gift from Dr. Theo J. Visser), both diluted at 1:1,000. The primary antisera were detected with Alexa Fluor 488-conjugated donkey anti-rabbit IgG diluted at 1:400 (Jackson Immunoresearch). Immunostaining with both antisera resulted in the same patterns reported earlier (26, 37).

Image analysis

In situ hybridization signals were compared between sections from a single hybridization experiment where all conditions and exposure times were identical. Darkfield images of OATP1c1 *in situ* hybridization were analyzed with ImageJ software (public domain at http://rsb.info.nih.gov/ij). To maximize the analysis of OATP1c1 signal in blood vessels, hybridizations were analyzed in the hypothalamus where no significant signal was detected in astrocytes after 9 days exposure in mice or 5

days exposure in rats. Images were taken with a 5× objective at the level of the paraventricular nucleus (mice) or the dorsomedial nucleus (rats), and integrated density values were calculated. From the two rat OATP1c1 hybridizations, only the 5 day exposure experiment was used for quantitative image analysis. Images from both the 9 and 5 days exposure experiments were used to illustrate the magnitude of changes in OATP1c1 hybridization signal. To quantify vascular MCT8 hybridization in mice, blood vessel segments with clear hybridization signal were counted in the thalamus and hypothalamus in 3 sections per mouse at the rostro-caudal level of the median eminence. In these regions, the low neuronal hybridization signal allowed easier identification of labeled blood vessels than in cortical regions. OATP1c1 immunofluorescence in blood vessels was quantified in rats using ImageJ. Images were taken with a 20× objective of an area with high density of blood vessels in the midline thalamus. The area covered by immunofluorescently labeled vessels (pixel number) was measured by subtracting non-labeled areas (i.e., dark pixels) from the image using the threshold tool and the same threshold value for all images. Hematoxylin and eosin staining was used to facilitate the identification of arachnoid veins in rats.

Statistical analysis

Data are presented as mean ± SEM. Quantitative PCR data were expressed as RQ (mean +/- SEM). Quantitative PCR data from cortex and image analysis data were compared between groups by one-way ANOVA and Newman-Keuls multiple comparison post-hoc test. Quantitative PCR data from the leptomeninges were compared by Student's t test.

Results

Effect of LPS on OATP1c1 expression in the brain

OATP1c1 mRNA. LPS administration similarly affected OATP1c1 expression in mice and rats. OATP1c1 mRNA levels decreased profoundly within 9h after LPS injection, as demonstrated by a striking reduction in hybridization signal across the forebrain (Fig. 1A, 1B). Emulsion autoradiography revealed that this reduction was due to a loss of hybridization signal specifically in blood vessels, but not

astrocytes. Vascular OATP1c1 expression decreased uniformly in the forebrain, but the course of this response could be followed most clearly in the hypothalamus (Fig. 2A) where hybridization signal in astrocytes was the lowest among forebrain regions. Hybridization signal in vessels decreased significantly as soon as 2h after LPS, and markedly by 4h (Fig. 2A). Vascular hybridization signal was virtually absent in mice 9h after LPS injection, except light labeling of the highly vascularized hypothalamic paraventricular nucleus (Fig. 2A). A similar reduction was observed in rats, where only scattered blood vessels with light hybridization signal were detected at 9h after LPS (in the hybridization experiment with the longer, 9 day autoradiography exposure). Moderate labeling remained only in some vessels of the paraventricular and supraoptic nuclei (Fig. 3A; also in Fig 1A); in fact, vessels in these two nuclei were more intensely labeled than elsewhere, even in control rats. The loss of OATP1c1 hybridization signal in blood vessels is also demonstrated in images from the cerebral cortex in Figs. 2B and 3A.

Hybridization signal in astrocytes did not change noticeably in either species, and remained comparable to control levels 9h after LPS, as demonstrated in images from the mouse and rat cortex (Fig. 2B, 3A). Notably, OATP1c1 mRNA in astrocytes varied greatly between brain regions, confirming recent studies (23, 27). In mice, OATP1c1 mRNA was easily detected in hippocampal and cortical astrocytes, while it was not detected in hypothalamic astrocytes with the exposure time used in this experiment. In rats, differences in astrocytic OATP1c1 expression were confirmed by both fluorescent (Fig. 3B) and radioactive *in situ* hybridization. Hybridization signal was moderate to intense in astrocytes of the cortex, hippocampus, striatum, and ventrolateral thalamus, whereas it was much lighter in astrocytes of the hypothalamus, such as in the ventromedial nucleus (Fig. 3B).

In both species, vascular OATP1c1 hybridization signal increased above control levels during the recovery phase from endotoxemia. In mice, OATP1c1 mRNA was still below control levels at 24h, but increased markedly at 48h after LPS (Fig. 2A). In rats, upregulation of OATP1c1 mRNA in blood vessels could be observed at both 24h and 48h after LPS (Fig. 3A). Conspicuously increased signal in vessels was observed in one out of four rats in the 24h LPS group, and three out of four rats in the 48h

LPS group. Markedly increased OATP1c1 mRNA at 24h after LPS was confirmed in another experiment (2 out of 2 rats; data not shown). This indicates that the timing of post-endotoxemic increase in vascular OATP1c1 mRNA can vary among individual rats. Image analysis results from mice and rats representing vascular OATP1c1 mRNA expression at each time point following LPS injection are presented in Fig. 4A. Quantitative RT-PCR data from cortical samples confirmed the in situ hybridization results, as OATP1c1 mRNA was significantly decreased 9h after LPS injection in both species (Fig. 4B). At 48h after LPS, OATP1c1 mRNA levels were not different from control levels by quantitative PCR (Fig. 4B). In the choroid plexus, OATP1c1 hybridization signal was consistently reduced 9h after LPS in mice (Fig. 1B), but not rats. In tanycytes, OATP1c1 mRNA expression was extremely intense in rats (Supplemental Fig. 1), but conspicuously absent in mice (Supplemental Fig. 2). LPS did not affect OATP1c1 expression in rat tanycytes.

OATP1c1 protein. Immunofluorescence for OATP1c1 gave clear labeling of blood vessels in the rat brain with low background, whereas in mice the labeling was less sensitive and less clear due to higher background levels. The antiserum did not label astrocytes. Immunostaining of blood vessels did not differ between control, 2h and 4h LPS groups, but visibly decreased at 9h and 24h (5A, 5B). At 24h, when the decrease was significant by image analysis (Fig. 4A), only scattered major vessel segments were labeled in both species (Fig. 5A, 5B). OATP1c1 immunostaining in vessels at 48h after LPS was similar to controls (Fig. 5A, 5B). OATP1c1 immunostaining was intense in rat tanycytes (Supplemental Fig. 1), whereas in mice it was observed selectively in lateral beta (beta-1) tanycytes in the floor of the third ventricle (Supplemental Fig. 2). The presence of OATP1c1 immunoreactivity in mouse tanycytes is in agreement with a previous report by Roberts et al. (26) that used highly specific antibodies.

Effect of LPS on MCT8 expression in the brain

MCT8 mRNA. LPS similarly affected MCT8 expression in mice and rats. The hybridization patterns in control brains were identical to what was previously described (25). Several neuronal populations were labeled with variable, light to intense signal, and scattered larger blood vessels were labeled with

moderate or light signal (Fig. 1C). Rat tanycytes were intensely labeled, and extremely intense signal labeled mouse tanycytes and the choroid plexus in both species (Fig. 1C). Neuronal MCT8 expression did not noticeably change at any time after LPS injection in both species (Fig. 1C). In contrast, MCT8 mRNA expression in blood vessels changed markedly in response to LPS. In mice, the intensity of vascular labeling decreased gradually from 2h until 9h, when hybridization signal was no longer detected in vessels (Fig. 6A). A similar trend was observed in rats, with noticeably less numerous and less intensely labeled blood vessels at 4h, and only occasional, lightly labeled vessels visible at 9h (Fig. 6B). In mice, both the number of detected vessel segments and their signal intensity increased at 24h after LPS compared to control mice, and even more strikingly at 48h (Fig. 1C, 6A). The quantification of labeled vessels in mice is presented in Fig. 4A. In rats, labeling of blood vessels was comparable to control levels at 24h, but increased markedly by 48h after LPS (Fig. 6B). Quantitative PCR from the mouse cortex did not detect significant changes in MCT8 mRNA after LPS (Fig. 4B). In the rat cortex, MCT8 mRNA tended to decrease at 9h albeit not significantly, but significantly increased 48h after LPS (Fig. 4B).

MCT8 protein. MCT8 immunolabeling in blood vessels was not different from control levels at 2, 4, 9 or 48h after LPS in both species. Only a slight decrease in labeling was observed at 24h in mice (Fig. 5C). Intense MCT8 immunofluorescence was observed in axons in both species, in accordance with our previous description of specific axonal MCT8 labeling (37). MCT8-containing axons were present in most brain regions, but unaffected by LPS.

Effect of LPS on OATP1c1, MCT8 and D2 mRNAs in the rat leptomeninges

Since we previously observed that LPS administration induces robust D2 expression in the leptomeninges of rats (15), we also studied the expression of TH transporters in this tissue. OATP1c1 mRNA-expressing cells were observed in arachnoid veins, but not arteries or in the arachnoid tissue itself (Fig. 7A). Following LPS, OATP1c1 hybridization signal could no longer be detected in the wall of the veins at 2, 4 or 9h later (Fig. 7A), but returned to control levels by 24h, and remained normal at 48h. Conversely, D2 mRNA was induced in the wall of the arachnoid veins but not arteries following LPS (Fig

7A), which we did not previously recognize (15). Moderate to intense MCT8 hybridization signal was observed in the leptomeningeal layers between the hippocampus and thalamus (Fig. 7A), and the dorsal third ventricle adjacent to the choroid plexus. This signal did not change significantly following LPS administration. MCT8 hybridization signal in the arachnoid covering the outer brain surface was uncertain, as control hybridizations with the sense transcript also yielded labeling in this location, although less intensely than the antisense probe. By quantitative PCR from leptomeninges removed from the basal forebrain, OATP1c1 mRNA was reduced to approximately 10% of control level 9h after LPS injection, MCT8 mRNA did not change, while D2 mRNA increased 86-fold on average (Fig. 7B).

Discussion

While data have been accumulating on cell-type specific regulation of TH action in the brain, regulation of TH transport is poorly understood. In the present study, regulation of TH transporters was studied in the forebrain using a model of non-thyroidal illness syndrome, a condition known to evoke marked changes in tissue TH availability (1, 2). In particular, we report changes in OATP1c1 and MCT8 expression in the rodent brain in response to LPS administration, with the following main findings: 1) OATP1c and MCT8 mRNAs decrease rapidly and robustly in blood vessels; 2) this effect is cell-type specific as OATP1c1 and MCT8 mRNA levels remain unaltered in astrocytes and neurons; 3) a robust decrease in OATP1c1 but not MCT8 protein levels in vessels follows hours later; 4) during recovery from endotoxemia, OATP1c1 and MCT8 mRNA levels increase markedly in blood vessels above control levels; 5) these changes occur in both mice and rats. In addition, we describe OATP1c1 expression in arachnoid veins but not arteries that respond to LPS in a similar way as parenchymal blood vessels, and MCT8 mRNA in part of the rat leptomeninges.

MCT8 and OATP1c1 have complementary functions in the blood-brain barrier, and work in tandem to allow TH access to the brain (24). The parallel changes in OATP1c1 and MCT8 mRNAs in brain vessels during endotoxemia further corroborates the functional link between these transporters, and suggest a common mechanism regulating the expression of these genes during inflammation. The mechanisms by

which rapid downregulation of both transporter mRNAs occurs is unknown, but could be a direct effect of cytokines or other associated inflammatory signals that are associated with endotoxin administration. However, this response was specific to cells comprising the brain vasculature, such as endothelial cells known to express these transporters (26, 34, 38) and possibly also pericytes, while OATP1c1 and MCT8 mRNA levels remained unchanged in astrocytes and neurons. One possibility to explain the latter phenomenon is that the extracellular signal that down-regulates MCT8 and OATP1c1 expression in vessels has limited access to astrocytes and neurons inside the blood-brain barrier. Alternatively, the signal may be present in the brain parenchyma, but due to intrinsic properties of astrocytes and neurons, has no effect on OATP1c1 or MCT8 mRNA. The latter might be explained by the lack of receptors for the signal molecule, or that the signaling pathway activated is not coupled to the mechanism that changes the transcription of the transporter genes.

The marked increase in OATP1c1 and MCT8 mRNAs during the recovery period from endotoxemia may be secondary to low intracellular TH levels in microvascular cells, supported by data that OATP1c1 in rat brain microvessels is upregulated by hypothyroidism (28). However, regulation of OATP1c1 and MCT8 mRNAs by TH was not observed in congenitally hypothyroid mice (25), raising the possibility that increased OATP1c1 and MCT8 mRNA expression may be a rebound effect independent of TH concentration.

At the protein level, OATP1c1 decreased in brain vessels in a similarly robust manner as OATP1c1 mRNA, but only several hours later. This delay likely reflects the turnover rate of OATP1c1 protein in cells of the blood-brain barrier. In contrast, only a modest decrease in vascular MCT8 immunostaining was observed in mice. A possible explanation is that the half-life of MCT8 may be substantially longer than that of OATP1c1, and in our model, the inflammatory state may have been too transitory to see a significant decrease in the MCT8 protein. Thus, an inflammation model of longer duration may be necessary to more definitively address whether MCT8 decreases similar to OATP1c1. Since our analysis did not provide information on the subcellular location of the transporters, it is also conceivable that

internalization of OATP1c1 and/or MCT8 from the cell membrane could result in a more rapid decrease in TH transport before a decrease in protein levels is realized.

Access of TH to most of the brain parenchyma primarily occurs *via* the blood-brain barrier, and much less via the blood-cerebrospinal fluid barrier (39). Since deficiency in either OATP1c1 or MCT8 is sufficient to reduce brain TH uptake (24, 32), downregulation of these transporters in brain vessels during inflammation suggests diminished TH uptake into the brain parenchyma and may contribute to common symptoms associated with illness such as fatigue, depressed mood, and impaired neurocognitive function. In support, a recent clinical study reported that certain OATP1c1 polymorphisms are associated with fatigue and depression in a population of patients with adequately treated hypothyroidism (40).

Inflammatory regulation of OATP1c1 and MCT8 was strikingly different from that observed for D2 that is highly inducible by the inflammatory transcription factor, nuclear factor-kappa B (NF-κB) (11, 41). LPS induces D2 *via* NF-κB in tanycytes (7, 15), and probably in meningeal fibroblasts (15). In contrast, OATP1c1 and MCT8 expression did not increase following LPS in any cell type in the brain, and markedly decreased in cells of brain blood vessels. The opposite regulation of D2 and OATP1c1/MCT8 by inflammation raises the possibility that during inflammation, TH availability may not be uniform throughout the brain. The downregulation of OATP1c1 and MCT8 at the blood-brain barrier suggests decreased TH availability within the brain parenchyma, whereas induction of D2 suggests increased TH availability in the leptomeninges and choroid plexus (15). Therefore, inflammation may result in both "hypothyroid" and "hyperthyroid" compartments in the rat brain. As we previously hypothesized (15), increased TH levels in the leptomeninges and choroid plexus, where the proinflammatory reaction is the most intense following LPS administration (42-47), may serve to control inflammatory processes and improve macrophage function (6, 8, 16-18). It can be also speculated, however, that at the same time decreased TH levels might be adaptive for cells in the brain parenchyma. While further research will be necessary to understand the pathophysiological role of these changes, the present findings underscore that TH availability may differ significantly for different cell types of a single organ during the non-thyroidal illness syndrome.

In conclusion, OATP1c1 and MCT8 expression is downregulated in the blood-brain barrier during inflammation, suggesting decreased TH uptake into the rodent brain. TH uptake studies in inflammation models will be essential in the future to test the importance of TH transporter downregulation on TH delivery to the brain.

Acknowledgements

We thank Dr. Theo Visser for generously providing the MCT8 and OATP1c1 antisera.

References

1. Boelen A, Kwakkel J, Fliers E 2011 Beyond low plasma T3: local thyroid hormone metabolism during inflammation and infection. Endocr Rev 32:670-693
2. Fekete C, Lechan RM 2014 Central regulation of hypothalamic-pituitary-thyroid axis under physiological and pathophysiological conditions. Endocr Rev 35:159-194
3. Van den Berghe G 2014 Non-Thyroidal Illness in the ICU: A Syndrome with Different Faces. Thyroid
4. Gereben B, Zavacki AM, Ribich S, Kim BW, Huang SA, Simonides WS, Zeold A, Bianco AC 2008 Cellular and molecular basis of deiodinase-regulated thyroid hormone signaling. Endocr Rev 29:898-938
5. Visser TJ 2013 Thyroid hormone transporters and resistance. Endocr Dev 24:1-10
6. Kwakkel J, Surovtseva OV, de Vries EM, Stap J, Fliers E, Boelen A 2014 A novel role for the thyroid hormone-activating enzyme type 2 deiodinase in the inflammatory response of macrophages. Endocrinology 155:2725-2734
7. de Vries EM, Kwakkel J, Eggels L, Kalsbeek A, Barrett P, Fliers E, Boelen A 2014 NFkappaB signaling is essential for the lipopolysaccharide-induced increase of type 2 deiodinase in tanycytes. Endocrinology 155:2000-2008

8. Barca-Mayo O, Liao XH, DiCosmo C, Dumitrescu A, Moreno-Vinasco L, Wade MS, Sammani S, Mirzapoiazova T, Garcia JG, Refetoff S, Weiss RE 2011 Role of type 2 deiodinase in response to acute lung injury (ALI) in mice. Proc Natl Acad Sci U S A 108:E1321-1329

9. Boelen A, Kwakkel J, Chassande O, Fliers E 2009 Thyroid hormone receptor beta mediates acute illness-induced alterations in central thyroid hormone metabolism. J Neuroendocrinol 21:465-472

10. Boelen A, Kwakkel J, Thijssen-Timmer DC, Alkemade A, Fliers E, Wiersinga WM 2004 Simultaneous changes in central and peripheral components of the hypothalamus-pituitary-thyroid axis in lipopolysaccharide-induced acute illness in mice. J Endocrinol 182:315-323

11. Fekete C, Gereben B, Doleschall M, Harney JW, Dora JM, Bianco AC, Sarkar S, Liposits Z, Rand W, Emerson C, Kacskovics I, Larsen PR, Lechan RM 2004 Lipopolysaccharide induces type 2 iodothyronine deiodinase in the mediobasal hypothalamus: implications for the nonthyroidal illness syndrome. Endocrinology 145:1649-1655

12. Kwakkel J, Chassande O, van Beeren HC, Wiersinga WM, Boelen A 2008 Lacking thyroid hormone receptor beta gene does not influence alterations in peripheral thyroid hormone metabolism during acute illness. J Endocrinol 197:151-158

13. Kwakkel J, van Beeren HC, Ackermans MT, Platvoet-Ter Schiphorst MC, Fliers E, Wiersinga WM, Boelen A 2009 Skeletal muscle deiodinase type 2 regulation during illness in mice. J Endocrinol 203:263-270

14. Ma SF, Xie L, Pino-Yanes M, Sammani S, Wade MS, Letsiou E, Siegler J, Wang T, Infusino G, Kittles RA, Flores C, Zhou T, Prabhakar BS, Moreno-Vinasco L, Villar J, Jacobson JR, Dudek SM, Garcia JG 2011 Type 2 deiodinase and host responses of sepsis and acute lung injury. Am J Respir Cell Mol Biol 45:1203-1211

15. Wittmann G, Harney JW, Singru PS, Nouriel SS, Reed Larsen P, Lechan RM 2014 Inflammation-inducible type 2 deiodinase expression in the leptomeninges, choroid plexus, and at brain blood vessels in male rodents. Endocrinology 155:2009-2019

16. Chen Y, Sjolinder M, Wang X, Altenbacher G, Hagner M, Berglund P, Gao Y, Lu T, Jonsson AB, Sjolinder H 2012 Thyroid hormone enhances nitric oxide-mediated bacterial clearance and promotes survival after meningococcal infection. PLoS One 7:e41445

17. Cheng AW, Bolognesi M, Kraus VB 2012 DIO2 modifies inflammatory responses in chondrocytes. Osteoarthritis Cartilage 20:440-445

18. Perrotta C, Buldorini M, Assi E, Cazzato D, De Palma C, Clementi E, Cervia D 2014 The thyroid hormone triiodothyronine controls macrophage maturation and functions: protective role during inflammation. Am J Pathol 184:230-247

19. Castro I, Quisenberry L, Calvo RM, Obregon MJ, Lado-Abeal J 2013 Septic shock non-thyroidal illness syndrome causes hypothyroidism and conditions for reduced sensitivity to thyroid hormone. J Mol Endocrinol 50:255-266

20. Rodriguez-Perez A, Palos-Paz F, Kaptein E, Visser TJ, Dominguez-Gerpe L, Alvarez-Escudero J, Lado-Abeal J 2008 Identification of molecular mechanisms related to nonthyroidal illness syndrome in skeletal muscle and adipose tissue from patients with septic shock. Clin Endocrinol (Oxf) 68:821-827

21. Mebis L, Debaveye Y, Ellger B, Derde S, Ververs EJ, Langouche L, Darras VM, Fliers E, Visser TJ, Van den Berghe G 2009 Changes in the central component of the hypothalamus-pituitary-thyroid axis in a rabbit model of prolonged critical illness. Crit Care 13:R147

22. Kinne A, Schulein R, Krause G 2011 Primary and secondary thyroid hormone transporters. Thyroid Res 4 Suppl 1:S7

23. Muller J, Heuer H 2014 Expression pattern of thyroid hormone transporters in the postnatal mouse brain. Front Endocrinol (Lausanne) 5:92

24. Mayerl S, Muller J, Bauer R, Richert S, Kassmann CM, Darras VM, Buder K, Boelen A, Visser TJ, Heuer H 2014 Transporters MCT8 and OATP1C1 maintain murine brain thyroid hormone homeostasis. J Clin Invest 124:1987-1999

25. Heuer H, Maier MK, Iden S, Mittag J, Friesema EC, Visser TJ, Bauer K 2005 The monocarboxylate transporter 8 linked to human psychomotor retardation is highly expressed in thyroid hormone-sensitive neuron populations. Endocrinology 146:1701-1706

26. Roberts LM, Woodford K, Zhou M, Black DS, Haggerty JE, Tate EH, Grindstaff KK, Mengesha W, Raman C, Zerangue N 2008 Expression of the thyroid hormone transporters monocarboxylate transporter-8 (SLC16A2) and organic ion transporter-14 (SLCO1C1) at the blood-brain barrier. Endocrinology 149:6251-6261

27. Schnell C, Shahmoradi A, Wichert SP, Mayerl S, Hagos Y, Heuer H, Rossner MJ, Hulsmann S 2013 The multispecific thyroid hormone transporter OATP1C1 mediates cell-specific sulforhodamine 101-labeling of hippocampal astrocytes. Brain Struct Funct

28. Sugiyama D, Kusuhara H, Taniguchi H, Ishikawa S, Nozaki Y, Aburatani H, Sugiyama Y 2003 Functional characterization of rat brain-specific organic anion transporter (Oatp14) at the blood-brain barrier: high affinity transporter for thyroxine. J Biol Chem 278:43489-43495

29. Tohyama K, Kusuhara H, Sugiyama Y 2004 Involvement of multispecific organic anion transporter, Oatp14 (Slc21a14), in the transport of thyroxine across the blood-brain barrier. Endocrinology 145:4384-4391

30. Wirth EK, Roth S, Blechschmidt C, Holter SM, Becker L, Racz I, Zimmer A, Klopstock T, Gailus-Durner V, Fuchs H, Wurst W, Naumann T, Brauer A, de Angelis MH, Kohrle J, Gruters A, Schweizer U 2009 Neuronal 3',3,5-triiodothyronine (T3) uptake and behavioral phenotype of mice deficient in Mct8, the neuronal T3 transporter mutated in Allan-Herndon-Dudley syndrome. J Neurosci 29:9439-9449

31. Dumitrescu AM, Liao XH, Weiss RE, Millen K, Refetoff S 2006 Tissue-specific thyroid hormone deprivation and excess in monocarboxylate transporter (mct) 8-deficient mice. Endocrinology 147:4036-4043

32. Trajkovic M, Visser TJ, Mittag J, Horn S, Lukas J, Darras VM, Raivich G, Bauer K, Heuer H 2007 Abnormal thyroid hormone metabolism in mice lacking the monocarboxylate transporter 8. J Clin Invest 117:627-635

33. Ceballos A, Belinchon MM, Sanchez-Mendoza E, Grijota-Martinez C, Dumitrescu AM, Refetoff S, Morte B, Bernal J 2009 Importance of monocarboxylate transporter 8 for the blood-brain barrier-dependent availability of 3,5,3'-triiodo-L-thyronine. Endocrinology 150:2491-2496

34. Mayerl S, Visser TJ, Darras VM, Horn S, Heuer H 2012 Impact of Oatp1c1 deficiency on thyroid hormone metabolism and action in the mouse brain. Endocrinology 153:1528-1537

35. Bianco AC, Anderson G, Forrest D, Galton VA, Gereben B, Kim BW, Kopp PA, Liao XH, Obregon MJ, Peeters RP, Refetoff S, Sharlin DS, Simonides WS, Weiss RE, Williams GR 2014 American thyroid association guide to investigating thyroid hormone economy and action in rodent and cell models. Thyroid 24:88-168

36. Wittmann G, Hrabovszky E, Lechan RM 2013 Distinct glutamatergic and GABAergic subsets of hypothalamic pro-opiomelanocortin neurons revealed by in situ hybridization in male rats and mice. J Comp Neurol 521:3287-3302

37. Kallo I, Mohacsik P, Vida B, Zeold A, Bardoczi Z, Zavacki AM, Farkas E, Kadar A, Hrabovszky E, Arrojo EDR, Dong L, Barna L, Palkovits M, Borsay BA, Herczeg L, Lechan RM, Bianco AC, Liposits Z, Fekete C, Gereben B 2012 A novel pathway regulates thyroid hormone availability in rat and human hypothalamic neurosecretory neurons. PLoS One 7:e37860

38. Grijota-Martinez C, Diez D, Morreale de Escobar G, Bernal J, Morte B 2011 Lack of action of exogenously administered T3 on the fetal rat brain despite expression of the monocarboxylate transporter 8. Endocrinology 152:1713-1721

39. Dratman MB, Crutchfield FL, Schoenhoff MB 1991 Transport of iodothyronines from bloodstream to brain: contributions by blood:brain and choroid plexus:cerebrospinal fluid barriers. Brain Res 554:229-236

40. van der Deure WM, Appelhof BC, Peeters RP, Wiersinga WM, Wekking EM, Huyser J, Schene AH, Tijssen JG, Hoogendijk WJ, Visser TJ, Fliers E 2008 Polymorphisms in the brain-specific thyroid hormone transporter OATP1C1 are associated with fatigue and depression in hypothyroid patients. Clin Endocrinol (Oxf) 69:804-811

41. Zeold A, Doleschall M, Haffner MC, Capelo LP, Menyhert J, Liposits Z, da Silva WS, Bianco AC, Kacskovics I, Fekete C, Gereben B 2006 Characterization of the nuclear factor-kappa B responsiveness of the human dio2 gene. Endocrinology 147:4419-4429

42. Elmquist JK, Breder CD, Sherin JE, Scammell TE, Hickey WF, Dewitt D, Saper CB 1997 Intravenous lipopolysaccharide induces cyclooxygenase 2-like immunoreactivity in rat brain perivascular microglia and meningeal macrophages. J Comp Neurol 381:119-129

43. Lacroix S, Feinstein D, Rivest S 1998 The bacterial endotoxin lipopolysaccharide has the ability to target the brain in upregulating its membrane CD14 receptor within specific cellular populations. Brain Pathol 8:625-640

44. Lacroix S, Rivest S 1998 Effect of acute systemic inflammatory response and cytokines on the transcription of the genes encoding cyclooxygenase enzymes (COX-1 and COX-2) in the rat brain. J Neurochem 70:452-466

45. Quan N, Whiteside M, Herkenham M 1998 Time course and localization patterns of interleukin-1beta messenger RNA expression in brain and pituitary after peripheral administration of lipopolysaccharide. Neuroscience 83:281-293

46. Nadeau S, Rivest S 1999 Effects of circulating tumor necrosis factor on the neuronal activity and expression of the genes encoding the tumor necrosis factor receptors (p55 and p75) in the rat brain: a view from the blood-brain barrier. Neuroscience 93:1449-1464

47. Nadeau S, Rivest S 1999 Regulation of the gene encoding tumor necrosis factor alpha (TNF-alpha) in the rat brain and pituitary in response in different models of systemic immune challenge. J Neuropathol Exp Neurol 58:61-77

Figure legends

Figure 1. X-ray film autoradiograms of isotopic *in situ* hybridizations for rat and mouse OATP1c1, and mouse MCT8. (A) OATP1c1 mRNA expression in the rat forebrain in the function of time following LPS injection. Hybridization signal decreases after LPS injection; at 4 and 9h, the remaining visible signal in the hypothalamic paraventricular and supraoptic nuclei is vascular, while in other regions, such as the hippocampus and cortex, is primarily astrocytic. (B) LPS has the same effect on OATP1c1 mRNA in mice as in rats. In mice, OATP1c1 mRNA decreases even in the choroid plexus at 9h. (C) MCT8 mRNA in the mouse brain following LPS administration. Neuronal labeling remains unchanged. The bottom panel shows magnified views of the diencephalic area, where several labeled blood vessels (arrowheads) are visible at 24h and 48h, but none at 9h after LPS. cp, choroid plexus; Hip, Hippocampus; PVH, hypothalamic paraventricular nucleus; tan, tanycytes; SO, supraoptic nucleus; VMH, hypothalamic ventromedial nucleus. Scale bars = 2mm.

Figure 2. (A) Darkfield emulsion autoradiography images demonstrate the time course of OATP1c1 mRNA expression (silver grain accumulation, white) in the mouse hypothalamus after LPS injection. Hybridization signal labeled only blood vessels but not astrocytes in the hypothalamus. The signal virtually disappears by 9h, when only light signal remains visible in the paraventricular nucleus (PVH). At 48h, OATP1c1 mRNA increases significantly. Scale bar = 200μm. (B) Combination of *in situ* hybridization for OATP1c1 (silver grains) and GFAP immunofluorescence (red) demonstrates that LPS did not affect OATP1c1 mRNA expression in astrocytes. Images were taken from the piriform cortex (control) and adjacent cortical amygdala (LPS). White arrows in the overlay images indicate astrocytes

with OATP1c1 hybridization signal, open arrows point to blood vessel segments. Note that hybridization signal labels vessel segments in the control, but not in LPS-injected brain. Scale bar = 50μm.

Figure 3. (A) Darkfield emulsion autoradiography images illustrate the effect of LPS on OATP1c1 mRNA in the rat brain. The decrease in OATP1c1 mRNA levels at 9h is demonstrated in hybridizations with longer exposure time, while shorter exposure was necessary to visualize the increase at 48h. The top panel shows the dramatic decrease of OATP1c1 mRNA in vessels of the hypothalamic paraventricular nucleus (PVH). Middle panel demonstrates the effect in the cortex, where hybridization in vessels is almost completely absent 9h after LPS, and the remaining signal labels predominantly astrocytes. Arrows indicate longer vessel segments in the control cortex. The bottom panel demonstrates the robust increase in OATP1c1 mRNA levels in blood vessels at 48h after LPS; images were taken from the hypothalamic dorsomedial nucleus. PVH, hypothalamic paraventricular nucleus. Scale bar = 100 μm. (B) Fluorescent *in situ* hybridization demonstrates OATP1c1 mRNA in different astrocyte populations in the rat. Hybridization on paraformaldehyde-perfused sections shows high levels of OATP1c1 mRNA (green) in astrocytes of the hippocampus, cortex, and striatum. Note the numerous intense green puncta denoting OATP1c1 mRNA in the cytoplasm and proximal processes of astrocytes, which were identified by immunofluorescence for GFAP (red). In contrast, more sensitive hybridization using fresh-frozen sections was necessary to detect OATP1c1 mRNA in hypothalamic astrocytes. In these cells, hybridization signal concentrated in only a few, 5-8, smaller sized puncta. Cell nuclei are labeled by the blue fluorescence of DAPI. Scale bar = 20 μm.

Figure 4. (A) Results of semiquantitative image analysis of OATP1c1 and MCT8 *in situ* hybridization, and OATP1c1 immunofluorescence. OATP1c1 hybridization signal was quantified in the hypothalamus and represents mRNA expression specifically in blood vessels, as astrocytes were not labeled with the used exposure times. In the mouse MCT8 *in situ* hybridization experiment, the number of labeled blood vessels were counted in the diencephalic area in 3 sections per mouse, and the average number of vessels

per section was calculated and presented in the graph. OATP1c1 immunofluorescence in rats was quantified in images taken from the thalamus by measuring the area (pixel number) covered by immunolabeled vessels. Sample sizes: 4 or 5 rats or mice/group. * $P < 0.05$; ** $P < 0.01$; *** $P < 0.001$ vs control. (B) Quantitative RT-PCR results from the mouse and rat cortex 9 and 48h after LPS injection. OATP1c1 mRNA is significantly reduced 9h after LPS injection in both species: In rats, MCT8 mRNA tended to decrease at 9h but did not reach significance (p= 0.07). Sample sizes: n=6 rats/group and 8 mice/group. * $P < 0.05$, *** $P < 0.001$ *vs* the corresponding controls.

Figure 5. (A) OATP1c1 immunofluorescence shows the time course of OATP1c1 protein in blood vessels of rats following LPS injection. Images were taken from the thalamus; note the decrease in labeling at 9h, and that only scattered vessel segments are labeled at 24h. (B) The same phenomenon is shown in mice in images taken from the rostral perifornical area. (C) MCT8 immunfluorescence in blood vessels of the mouse thalamus; labeling intensity is only mildly reduced at 24h after LPS. Scale bar = 50 μm.

Figure. 6. (A) Darkfield emulsion autoradiography images demonstrate the effect of LPS on MCT8 mRNA in brain blood vessels. Images were taken from the thalamus where labeled vessels (arrows) stand out due to virtually undetectable hybridization signal in neurons. The vascular signal vanishes completely by 9h after LPS. At 24h, and especially at 48h, more intense hybridization signal labels a higher number of vessels. Scale bar = 200 μm. (B) A similar phenomenon is illustrated in images taken from the rat hippocampus. At 9h after LPS only occasional vessels with faint hybridization signal were detected, while several vessels with intense signal were observed at 48h. Scale bar = 100 μm.

Figure 7. (A) *In situ* hybridization for OATP1c1, MCT8 and D2 in the rat leptomeninges. Red fluorescent cresyl violet counterstaining is overlaid on darkfield emulsion autoradiography images to help identify tissue locations (OATP1c1 and D2 images). Top: OATP1c1 mRNA is expressed specifically in

the wall of veins (v) that run in the arachnoid, but not in arteries (a), or the arachnoid tissue itself. Labeling of veins is absent 9h after LPS injection. Bottom left: MCT8 mRNA is expressed in the leptomeningeal layers between the hippocampus and thalamus (arrows). Bottom right: D2 mRNA is expressed in both the arachnoid tissue and wall of arachnoid veins (v), but not arteries (a) 9h after LPS injection. a, artery; opt, optic tract; SO, supraoptic nucleus; v, vein. Scale bar = 100μm in top, 200μm in bottom panels. (B) Quantitative RT-PCR results from rat leptomeningeal samples obtained from 6 control and 8 LPS-treated rats. OATP1c1 mRNA decreases to 10% of control value, while D2 increases ~86-fold on average. * $P < 0.05$; *** $P < 0.0001$ vs control.

Fig 1

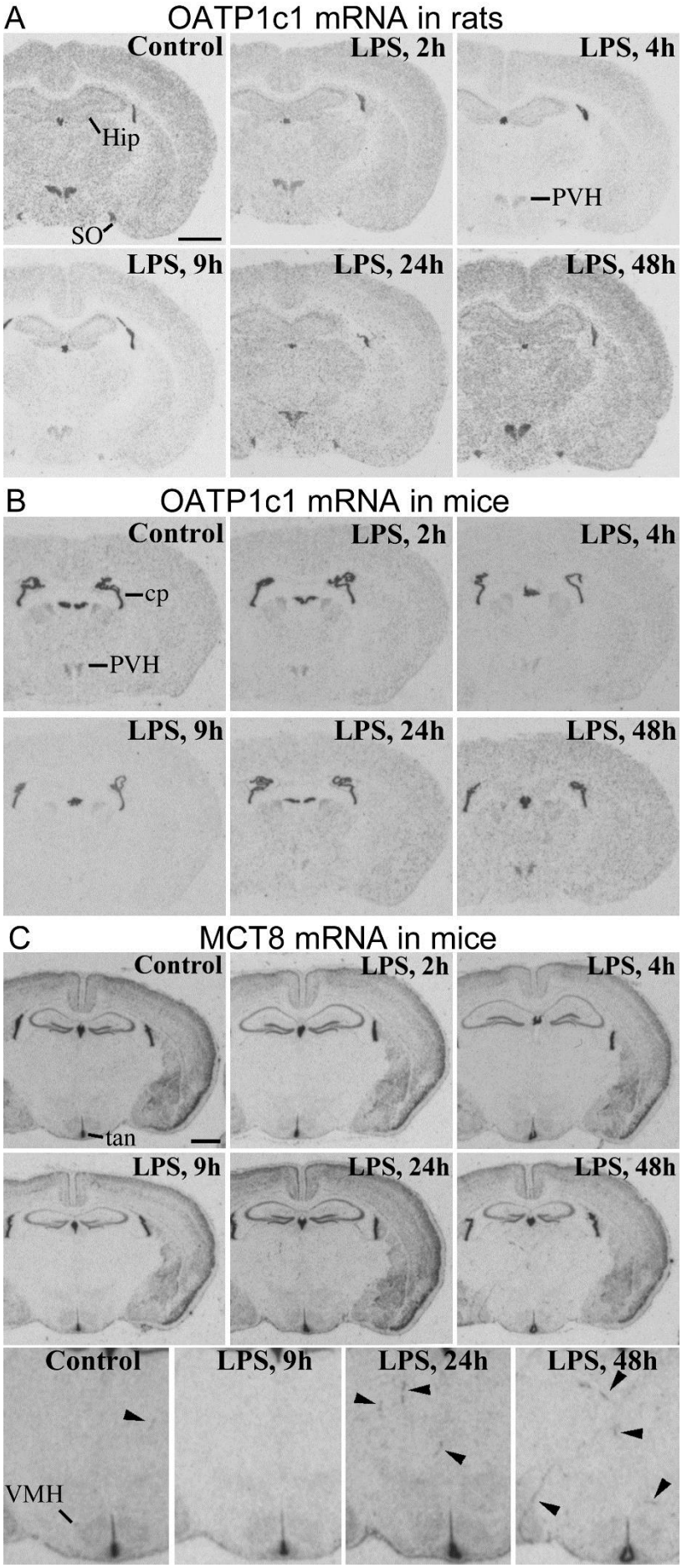
A
OATP1c1 mRNA in rats
Control
LPS, 2h
LPS, 4h
Hip
SO
PVH
LPS, 9h
LPS, 24h
LPS, 48h
B
OATP1c1 mRNA in mice
Control
LPS, 2h
LPS, 4h
cp
PVH
LPS, 9h
LPS, 24h
LPS, 48h
C
MCT8 mRNA in mice
Control
LPS, 2h
LPS, 4h
tan
LPS, 9h
LPS, 24h
LPS, 48h
Control
LPS, 9h
LPS, 24h
LPS, 48h
VMH

Fig 2

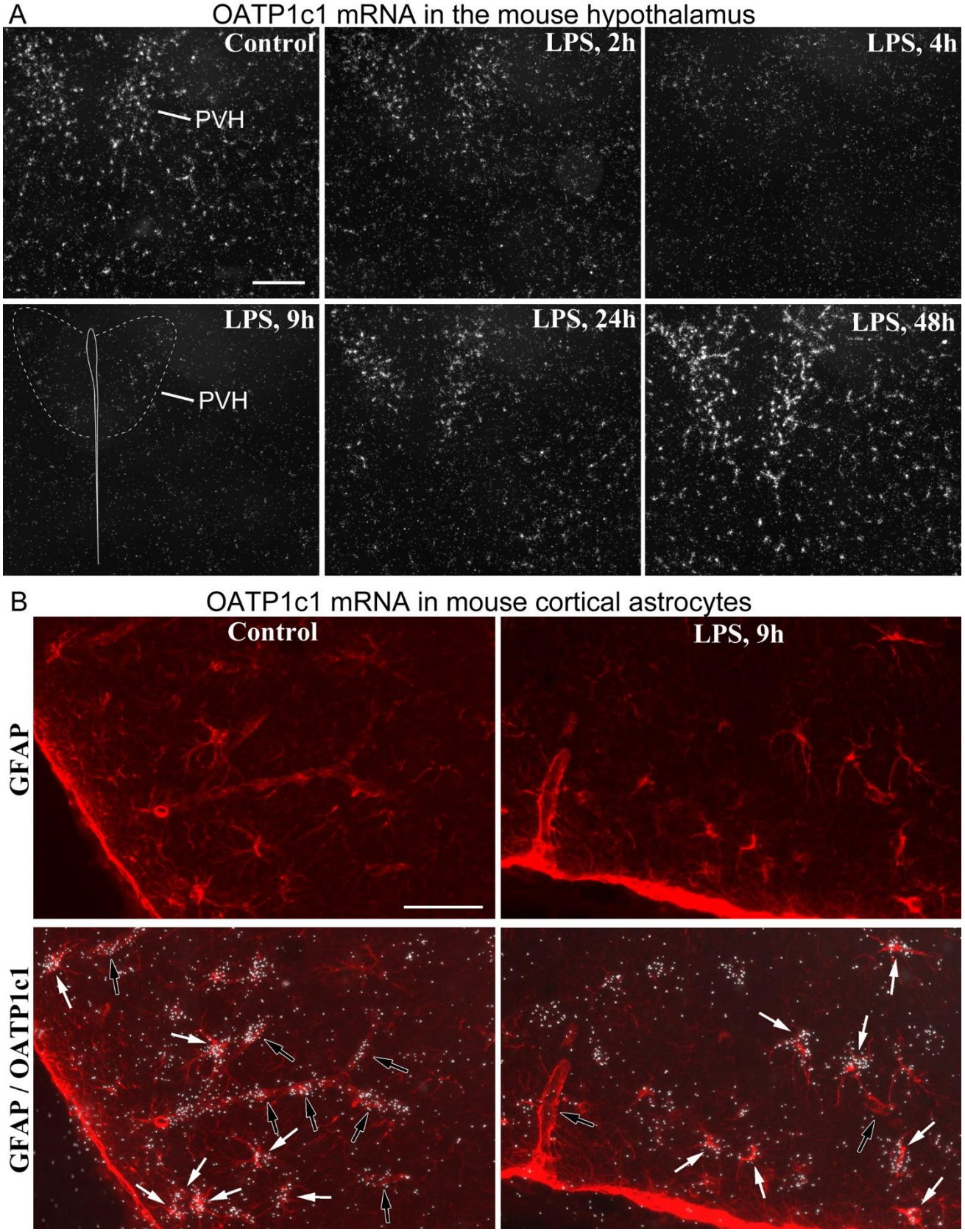
A
OATP1c1 mRNA in the mouse hypothalamus
Control
LPS, 2h
LPS, 4h
PVH
LPS, 9h
LPS, 24h
LPS, 48h
PVH
B
OATP1c1 mRNA in mouse cortical astrocytes
Control
LPS, 9h
GFAP
GFAP / OATP1c1

Fig 3

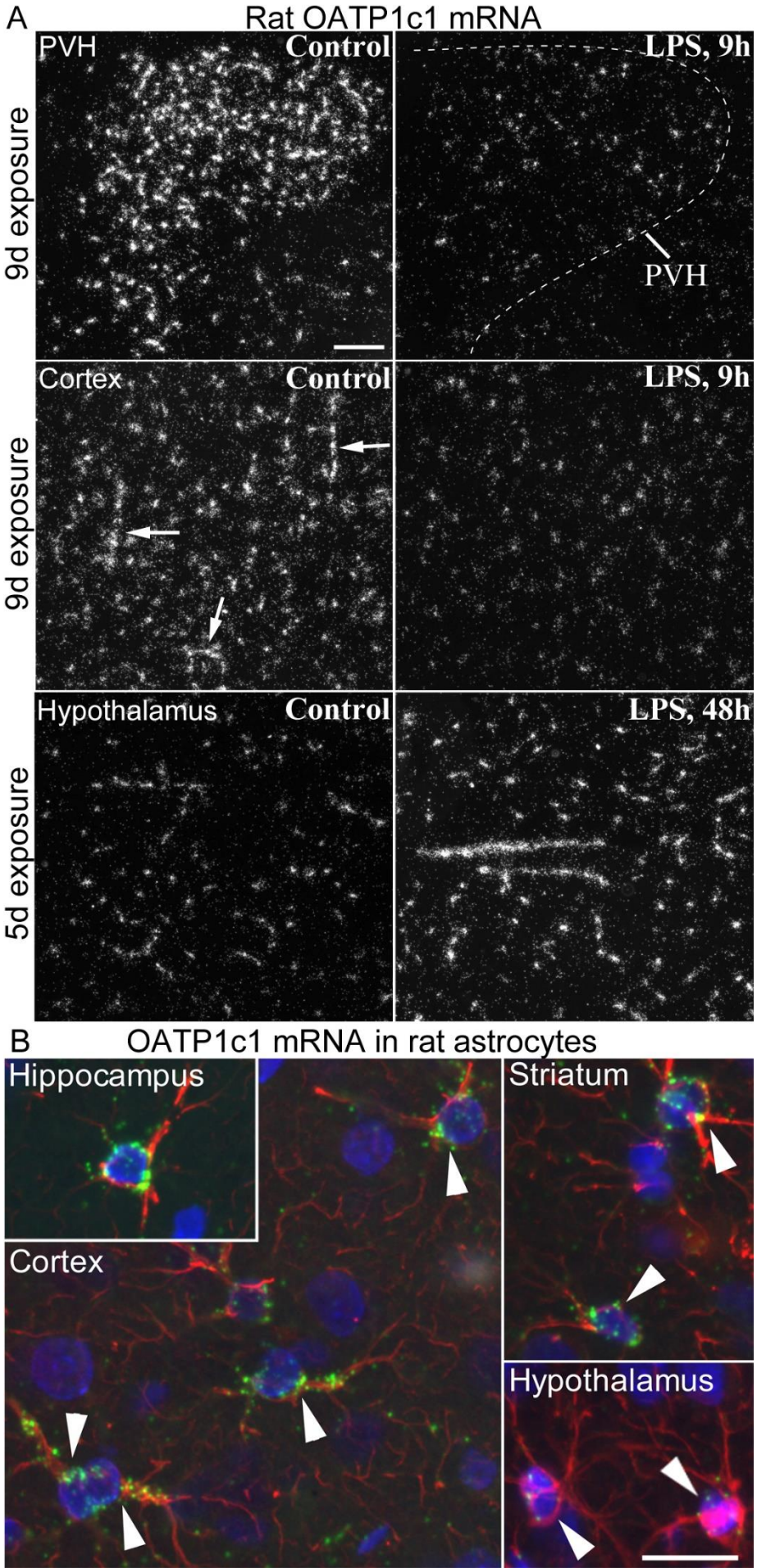
A
Rat OATP1c1 mRNA
PVH
Control
LPS, 9h
PVH
9d exposure
Cortex
Control
LPS, 9h
9d exposure
Hypothalamus
Control
LPS, 48h
5d exposure
B
OATP1c1 mRNA in rat astrocytes
Hippocampus
Striatum
Cortex
Hypothalamus

Fig 4

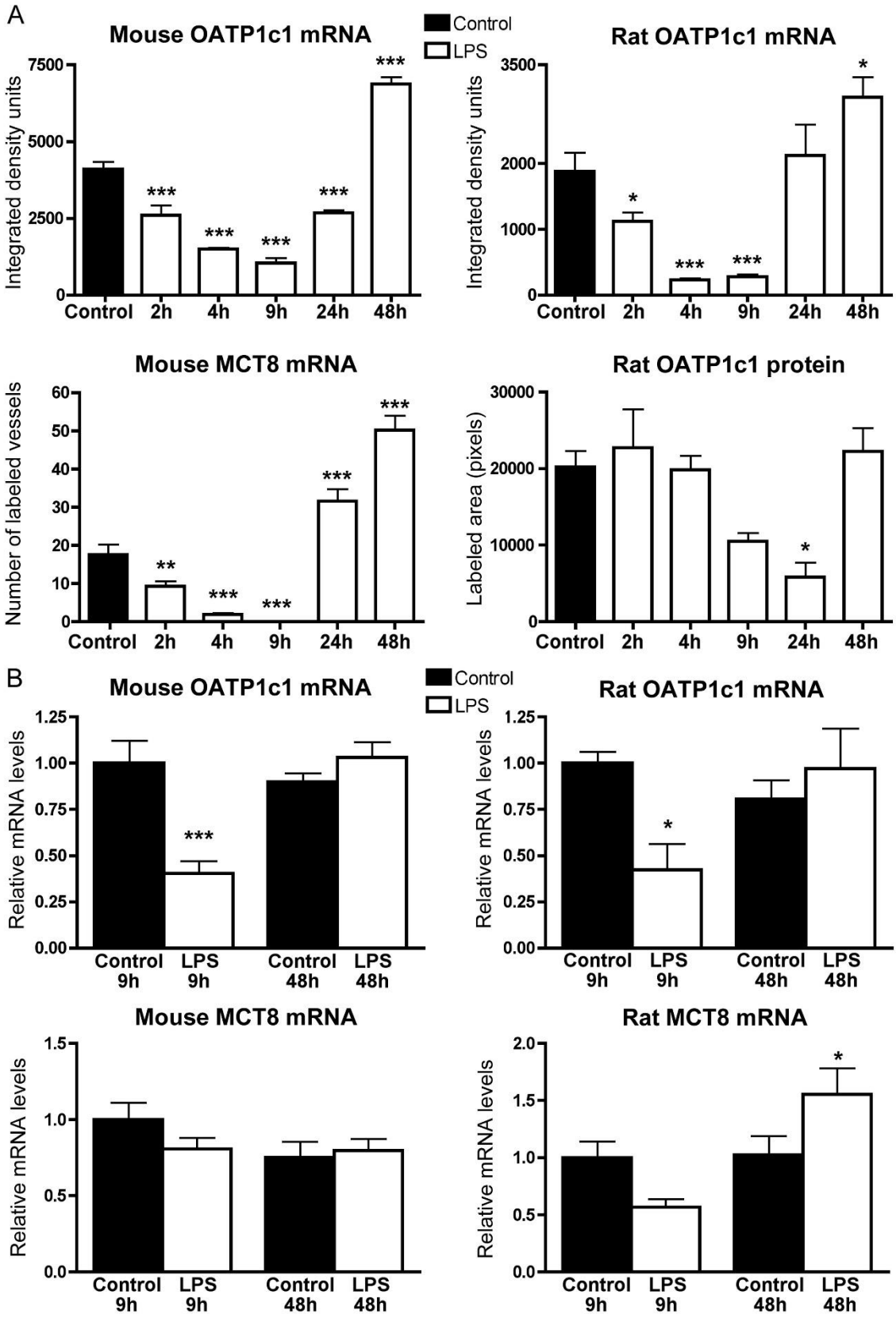
A
Mouse OATP1c1 mRNA
Control
LPS
Integrated density units
7500
5000
2500
0
Control 2h 4h 9h 24h 48h
Rat OATP1c1 mRNA
3500
2000
1000
0
Mouse MCT8 mRNA
Number of labeled vessels
60
50
40
30
20
10
0
Rat OATP1c1 protein
Labeled area (pixels)
30000
20000
10000
0
B
Mouse OATP1c1 mRNA
Rat OATP1c1 mRNA
Relative mRNA levels
1.25
1.00
0.75
0.50
0.25
0.00
Control 9h
LPS 9h
Control 48h
LPS 48h
Mouse MCT8 mRNA
Rat MCT8 mRNA
1.5
1.0
0.5
0.0
2.0
1.5

Fig 5

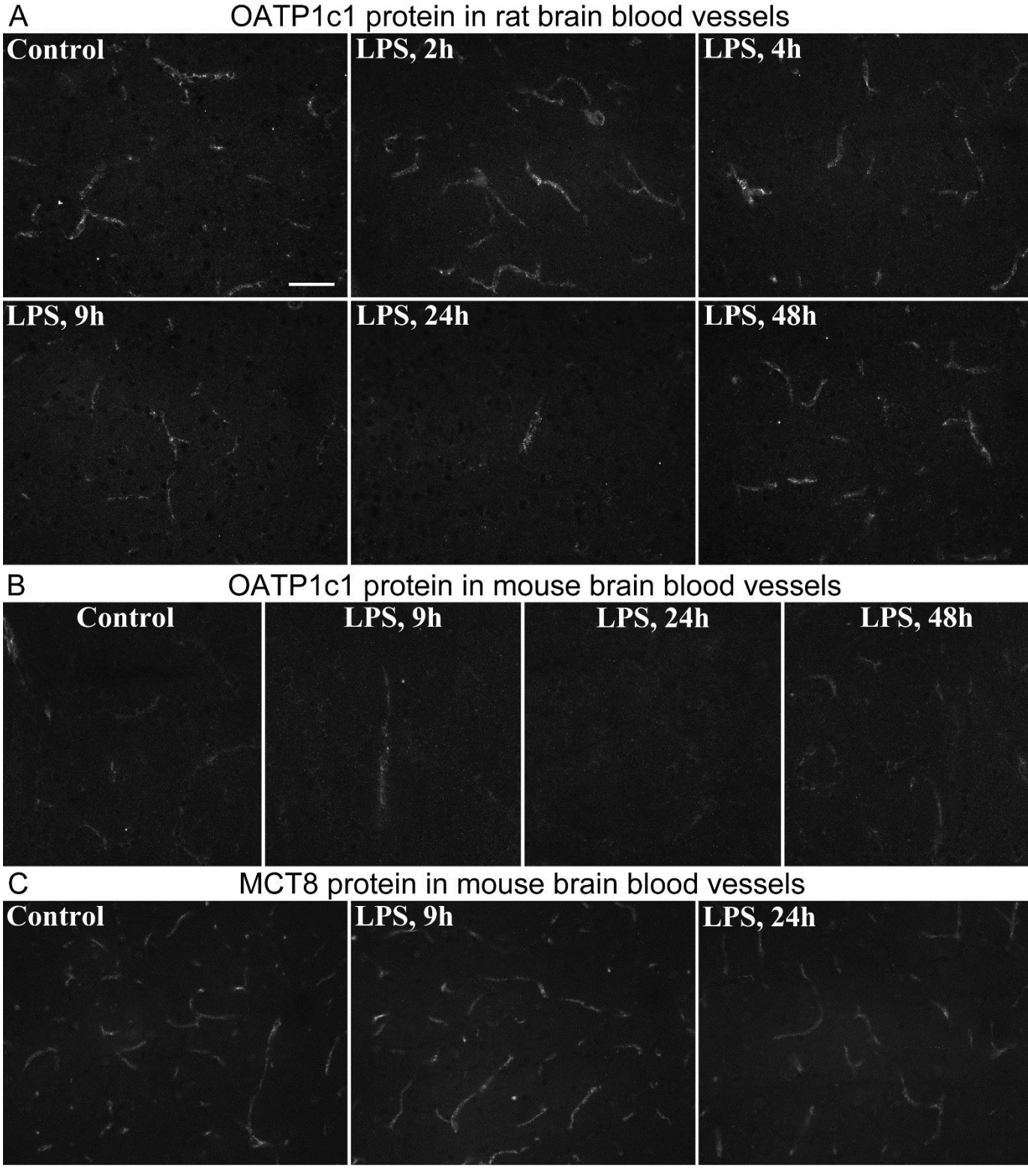
A
OATP1c1 protein in rat brain blood vessels
Control
LPS, 2h
LPS, 4h
LPS, 9h
LPS, 24h
LPS, 48h
B
OATP1c1 protein in mouse brain blood vessels
Control
LPS, 9h
LPS, 24h
LPS, 48h
C
MCT8 protein in mouse brain blood vessels
Control
LPS, 9h
LPS, 24h

Fig 6

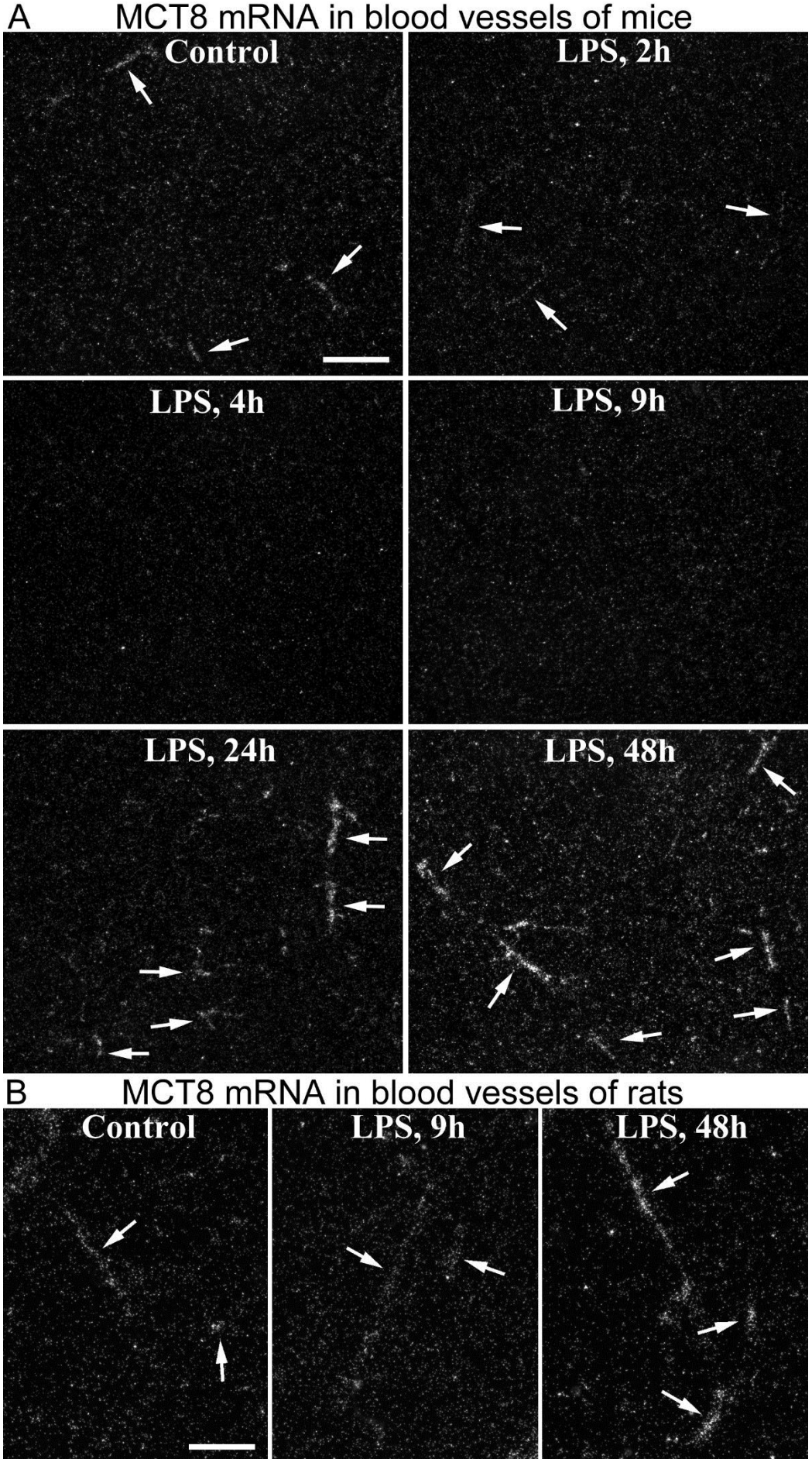
A
MCT8 mRNA in blood vessels of mice
Control
LPS, 2h
LPS, 4h
LPS, 9h
LPS, 24h
LPS, 48h
B
MCT8 mRNA in blood vessels of rats
Control
LPS, 9h
LPS, 48h

Fig 7

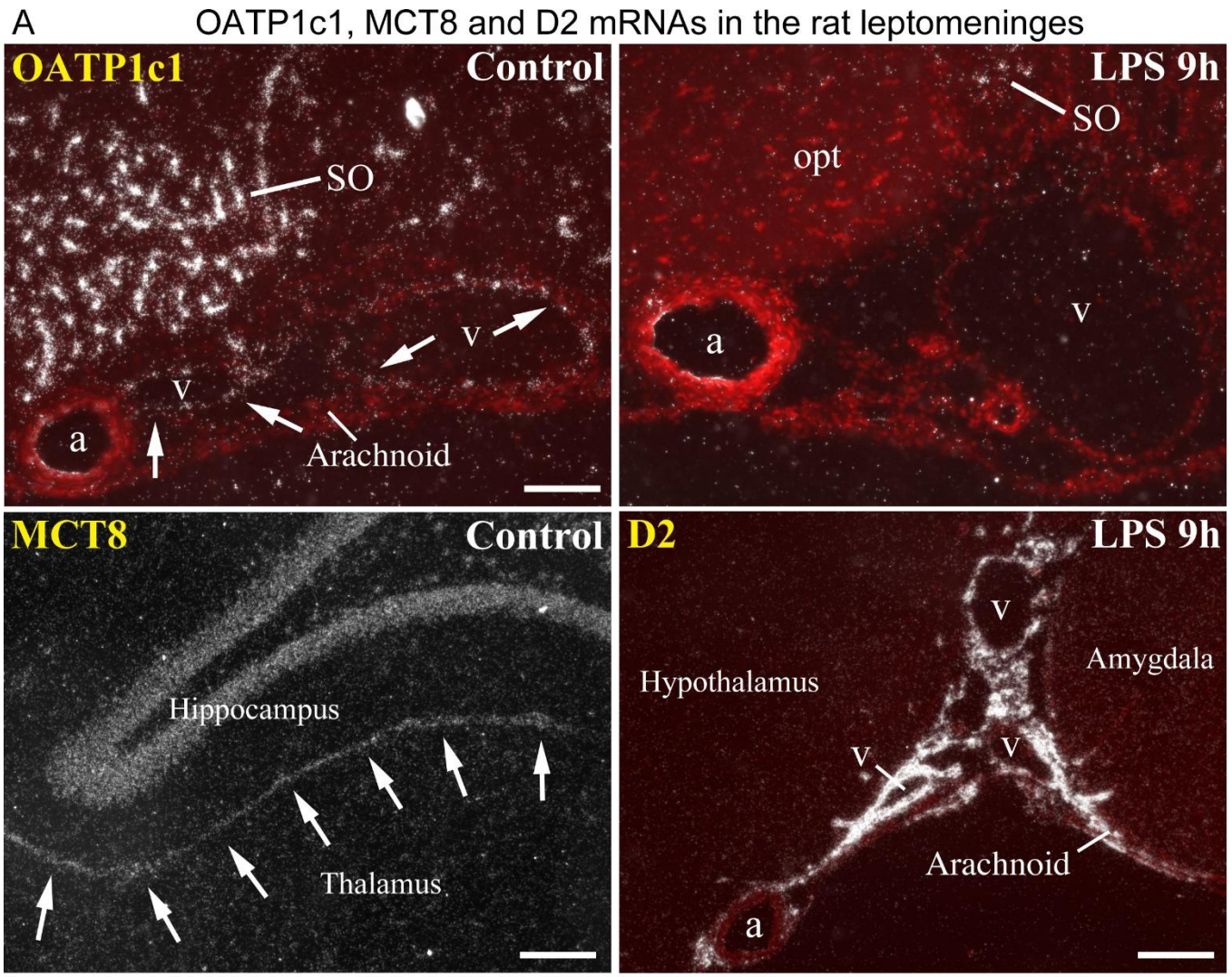
A
OATP1c1, MCT8 and D2 mRNAs in the rat leptomeninges
OATP1c1
Control
SO
v
v
a
Arachnoid
LPS 9h
SO
opt
v
a
MCT8
Control
Hippocampus
Thalamus
D2
LPS 9h
v
Hypothalamus
Amygdala
v
v
Arachnoid
a

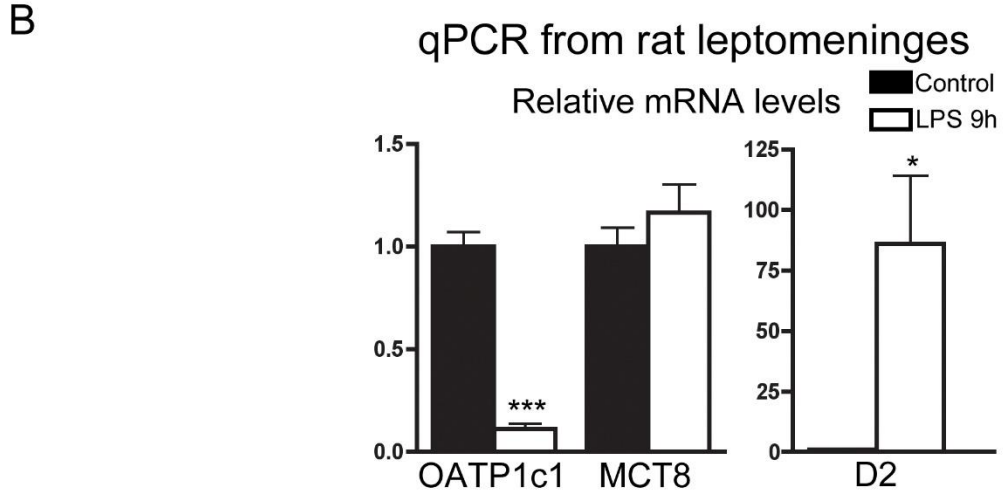
B
qPCR from rat leptomeninges
Relative mRNA levels
Control
LPS 9h
1.5
1.0
0.5
0.0
***
OATP1c1
MCT8
125
100
75
50
25
0
*
D2